On Amplitude Estimation for High-Speed Atomic Force Microscopy

Michael R. P. Ragazzon[1], J. Tommy Gravdahl[1], Andrew J. Fleming[2]

***Abstract*— Amplitude estimation or demodulation plays a vital part in the control loop of dynamic mode high-speed atomic force microscopy (AFM). The closed-loop bandwidth will be limited by the convergence speed of the estimator. Recent developments have introduced new ways of demodulating the measured deflection signal. This article reviews and compares present methods for AFM amplitude demodulation and introduces a new Lyapunov based estimator. The performance of the techniques are discussed in terms of bandwidth, measurement noise, convergence time, unwanted harmonics, and complexity.**

I. INTRODUCTION

Atomic force microscopy (AFM) [1] is a tool capable of studying and manipulating matter down to the atomic scale. This has made it one of the fundamental tools within the field of nanotechnology.

Dynamic modes of AFM [2] are often used for imaging the sample. In these modes the cantilever is oscillated using a dither piezo located at the base of the cantilever. Typically the amplitude, phase or frequency of the cantilever deflection is used in a feedback loop. In amplitude modulated (AM) mode the amplitude is compared to a setpoint which is kept constant by the controller as shown in Figure 1. By maintaining constant amplitude the distance to the sample remains constant, this is achieved by adjusting a vertically oriented z-piezoscanner. The z-scanner position can then be recorded as the sample is scanned in a raster pattern along the lateral directions to produce a topography map of the sample. Other ways of imaging in dynamic mode include detecting the interaction force directly [3] or the tip-sample distance itself [4].

Increasing the imaging rate has been an enduring ambition in the AFM community [5]. Several strategies have been performed for increasing the imaging rate ranging from improvements to mechanical design [6], virtually controlling the stiffness of the cantilever with active Q-control [7], [8], to improving the feedback controller [9].

AM-mode is well suited for imaging biological samples since the interaction forces generated can be very small, preventing damage to the sample [10]. However, AM-mode has generally been slower than traditional contact mode. By increasing the bandwidth of the amplitude estimator it is possible to increase the bandwidth of the entire closed-loop system and ultimately allow for faster imaging speeds. Additionally, by improving the estimator's noise response and attenuation of unwanted frequency components the resulting image will be improved.

Traditionally, amplitude estimation has been performed by peak-detection or lock-in amplifier techniques requiring up to ten oscillation cycles to converge. The high-speed AFM results presented in [11] introduces the much faster peak hold method which converges in half an oscillation cycle. However, this method is prone to noise and disturbances from unwanted harmonics. Recent developments include the high-bandwidth lock-in amplifier [12], Kalman filter [13], [14], and low-latency coherent demodulator [15].

In this paper traditional online amplitude estimation methods will be compared to recent developments in the field. Using these results and a properly defined set of performance indicators, recommendations are provided on the most suitable method for various application scenarios.

Additionally, a new method for amplitude estimation in AFM is proposed. To the authors' knowledge this estimation technique has not previously been employed in the AFM field. This Lyapunov based method has comparable bandwidth and noise response properties to the state-of-art amplitude estimators while being simpler to implement.

The paper is organized as follows. In Section II the amplitude estimation problem is presented and performance indicators for comparing such estimators are suggested. Section III introduces the various estimation techniques that have been implemented for comparison. In Section IV simulation results are presented. Considering these results the proper choice of a method for various scenarios is discussed in Section V. Section VI discusses some limitations for amplitude estimation before concluding in Section VII.

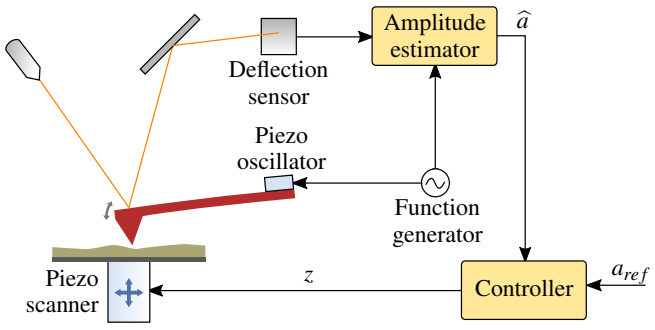

Fig. 1: Amplitude modulated operating mode in AFM.

[1] M. R. P. Ragazzon and J. T. Gravdahl are with the Department of Engineering Cybernetics, Norwegian University of Science and Technology, Trondheim, Norway. E-mail: ragazzon@itk.ntnu.no, Tommy.Gravdahl@itk.ntnu.no

[2] A. J. Fleming is with the School of Electrical Engineering and Computer Science, University of Newcastle, Callaghan, N.S.W. 2308, Australia. E-mail: andrew.fleming@newcastle.edu.au

II. PROBLEM FORMULATION

The goal is to estimate the unknown amplitude $a(t)$ considering the measured time-varying signal

$$s(t) = a(t)\sin(\omega_0 t + \phi) + w(t), \tag{1}$$

where ω_0 is the known angular frequency, ϕ is the unknown phase contribution, and $w(t)$ is a zero-mean Gaussian white noise process with covariance σ^2.

The following performance indicators are emphasized in this paper for comparing the various methods:

Bandwidth In dynamic mode high-speed AFM applications every part of the closed-loop cycle must maintain a large bandwidth including the amplitude estimator. This can be determined from the magnitude response plotted against frequency of sinusoidal input signals.

Convergence time The various estimation schemes are very different in their behavior, and due to the nonlinearity of the problem the magnitude plot needs to be supplemented with a description of qualitative behavior. Some methods converge in finite time, others in exponential time. This will be discussed in addition to a helpful step-response plot.

Bias and standard deviation Measurement noise is a limiting factor in the resolution of the deflection measurement and is dominated by thermal noise [16]. In addition to providing the bias and standard deviation after applying measurement noise, the response of the various methods to such noise can be plotted against frequency in a spectral density plot [17].

Higher-harmonics Due to the nonlinear nature of the interaction force between the cantilever and sample while imaging, other frequencies than the known oscillation frequency will be excited. This will excite the higher harmonics of the cantilever dynamics and can ultimately affect the resulting amplitude estimate.

Complexity Since speed is emphasized in AFM the complexity must be kept low enough for the method to be implementable. Some methods can be implemented in simple analog circuits while others require digital implementations with computationally demanding arithmetics. In general, by using a simpler method the sample rate can be increased, which will reduce the overall noise floor of the system [18].

III. AMPLITUDE ESTIMATION TECHNIQUES

In this section traditional and recent methods for amplitude estimation will be briefly introduced, with emphasis on those used in the AFM field. The purpose here is to introduce their mode of operation, while comparisons are discussed later in this paper. All methods are implementable online, preferably with short convergence time. Traditional offline amplitude estimation methods such as least squares [19] are not suitable for feedback control and are not discussed here. Note that the naming convention for the various methods is not consistent across the literature.

Notation

For the sake of clarity methods are described in either a continuous or discrete form depending on their most suitable method of implementation. Discrete signals are written as u_k, defined by

$$u_k \triangleq u(kT_s) = u(t), \quad \text{for } kT_s \le t < (k+1)T_s \tag{2}$$

where T_s is the sample time. Discrete filters are denoted using the z-transform transfer function $H(z)$ while continuous filters are described by a transfer function $H(p)$ where p is the Laplace-variable. Furthermore, the amplitude estimate is given by $\widehat{a}(t)$, a vector is written as lower-case bold ($\mathbf{x}$) and a matrix as upper-case bold ($\mathbf{A}$).

Quadrature Based Methods

Before presenting the various methods, a concept shared among several techniques will be introduced here. These amplitude estimation methods are based on the multiplication of an in-phase and a quadrature sinusoidal signal

$$s(t) = a(t)\sin(\omega_0 t + \phi) + w(t) \tag{3}$$
$$I(t) = s(t)\sin(\omega_0 t) \tag{4}$$
$$Q(t) = s(t)\cos(\omega_0 t). \tag{5}$$

By disregarding the noise term for now by setting $w = 0$, the following relations can be found using trigonometric identities

$$I(t) = \tfrac{a}{2}\left[\cos\phi - \cos(2\omega_0 t + \phi)\right] \tag{6}$$
$$Q(t) = \tfrac{a}{2}\left[\sin\phi + \sin(2\omega_0 t + \phi)\right]. \tag{7}$$

By attenuating or removing the $2\omega_0$ contribution in (6)-(7), the amplitude can easily be recovered from

$$i(t) \approx \tfrac{a}{2}\cos\phi \tag{8}$$
$$q(t) \approx \tfrac{a}{2}\sin\phi \tag{9}$$
$$\widehat{a}(t) = 2\sqrt{i(t)^2 + q(t)^2} \approx a(t). \tag{10}$$

A. Peak Detection

Peak detection is possibly the simplest method to implement. It can be constructed using a rectifier circuit and a low-pass filter [5]. It is characterized by slowly and continuously reducing its estimate, and then quickly rising as the measured signal becomes larger than the current estimate. The method can be written as

$$x_k = \max\left(s_k, \widehat{a}_{k-1}\right) \tag{11}$$
$$\widehat{a}_k = H_{lp}(z)x_k, \tag{12}$$

where $H_{lp}(z)$ is a low-pass filter with gain $0 \ll K < 1$.

B. RMS-to-DC

The root-mean-square (RMS) of a sinusoidal signal is correlated with the amplitude according to $a = \sqrt{2}v_{rms}$. Both analog and digital implementations are commercially

available. These solutions are typically made to remove DC-offset. Our implementation is given by

$$\widehat{a}_k = \sqrt{\frac{2}{MN}\sum_{n=0}^{MN} s_{k-n}^2}, \tag{13}$$

where N is the number of samples in one period and M is the number of periods. The choice of M will be a trade-off between convergence time and noise attenuation.

C. Peak Hold

This method was presented in [11] to enable high-speed imaging in dynamic mode AFM. The signal is sampled as it reaches its peak, allowing one or even two samples per oscillation period. It works by introducing a 90° phase-delay to the measured signal which is then used to trigger a sample and hold. The method can be described by

$$x_k = \mathrm{SH}(|s_k|, s_{k\perp}) \tag{14}$$
$$\widehat{a}_k = H_{lp}(z)x_k, \tag{15}$$

where $s_{k\perp}$ is a 90° phase-shifted version of s_k, $\mathrm{SH}(\cdot,\cdot)$ is a sample and hold function where the first argument is the output and the second argument triggers a new sample on crossing zero, and $H_{lp}(z)$ is a high-bandwidth low-pass filter used to smooth out the noise from the triggering.

D. Coherent Demodulator

This is a quadrature based method utilizing the definite integral of $I(\cdot), Q(\cdot)$ from (6)-(7) over one or multiple periods to remove the $2\omega_0$ frequency component,

$$i(t) = \int_{t-T_0}^{t} I(\tau)d\tau \tag{16}$$
$$q(t) = \int_{t-T_0}^{t} Q(\tau)d\tau \tag{17}$$
$$\widehat{a}(t) = 2\sqrt{i(t)^2 + q(t)^2}. \tag{18}$$

Accurate knowledge of the oscillation period and timing is required. In [15] these equations are implemented using the trapezoidal integration method. This technique is also referred to as the Fourier method [20] as it is equivalent to determining the first coefficients from the Fourier series.

E. Lock-in Amplifier

The second quadrature-based method uses a low-pass filter with bandwidth $\omega_c \ll \omega_0$ to suppress the frequency component at $2\omega_0$ from (6)-(7). It is simpler to implement than the coherent demodulator since accurate timing is not needed and it can be implemented using analog circuitry, but it is severely limited in terms of bandwidth. The method is given as

$$i_k = H_{lp}(z)I_k \tag{19}$$
$$q_k = H_{lp}(z)Q_k \tag{20}$$
$$\widehat{a}_k = 2\sqrt{i_k^2 + q_k^2}, \tag{21}$$

where $H_{lp}(z)$ is a low-pass filter with unit gain and bandwidth $\omega_c \ll \omega_0$.

F. High-Bandwidth Lock-in Amplifier

The bandwidth of the lock-in amplifier is severely limited by the $2\omega_0$ frequency-components contributions seen in (6)-(7), as this requires a low-pass filter with a bandwidth significantly lower than the oscillation frequency in order to attenuate these components. The high-bandwidth lock-in amplifier was introduced in [12] where the $2\omega_0$ components are eliminated by phase cancellation allowing for a much larger bandwidth on the low-pass filter.

A 90° phase-shift is introduced to the measured signal s, denoted by $s_\perp$. This is equivalent to switching the $\sin(\cdot)$ with a $\cos(\cdot)$ in (3). By repeating the steps of (3)-(7) with the phase-shifted signal $s_\perp$ the relations

$$I_\perp = \tfrac{a}{2}\left[\sin(2\omega_0 t + \phi) - \sin\phi\right] \tag{22}$$
$$Q_\perp = \tfrac{a}{2}\left[\cos(2\omega_0 t + \phi) + \cos\phi\right] \tag{23}$$

are found, where the time-dependency has been dropped for simplicity. By phase cancellation and trigonometric identities this results in

$$I + Q_\perp = a\cos(\phi) \tag{24}$$
$$Q - I_\perp = a\sin(\phi) \tag{25}$$
$$\widehat{a} = \sqrt{(I+Q_\perp)^2 + (I_\perp - Q)^2} = a. \tag{26}$$

In practice the phase-cancellation will not be perfect and a low-pass filter is still necessary to remove the resulting residues. However, these residues will be severely reduced compared to the lock-in amplifier which allows for a much greater bandwidth on the low-pass filter.

G. Kalman Filter

Recent studies have investigated the use of a Kalman filter for amplitude estimation [13], [14] with promising results. The states are modeled as the amplitude of in-phase and quadrature sinusoidal signals. The state-space model is given by

$$\mathbf{x}_k = \mathbf{x}_{k-1} + \mathbf{w}_{k-1} \tag{27}$$
$$\mathbf{c}_k = [\sin(\omega_0 k T_0), \cos(\omega_0 k T_0)] \tag{28}$$
$$y_k = \mathbf{c}_k\mathbf{x}_k + v_k \tag{29}$$

where $\mathbf{x}_k$ is the state vector, $y_k = s_k$ is the measured variable, $\mathbf{w}_k$ is white noise with covariance $\mathbf{Q}$ essentially describing how fast the amplitude changes, and v_k is white measurement noise with covariance $\mathbf{R}$.

The usual Kalman filter equations [21] are used for estimation of the states, rewritten here for convenience and simplified for the problem at hand:

$$\mathbf{x}_k^- = \mathbf{x}_{k-1} \tag{30}$$
$$\mathbf{P}_k^- = \mathbf{P}_{k-1} + \mathbf{Q} \tag{31}$$
$$\mathbf{K}_k = \mathbf{P}_k^-\mathbf{c}_k^T(\mathbf{c}_k\mathbf{P}_k^-\mathbf{c}_k^T + \mathbf{R})^{-1} \tag{32}$$
$$\mathbf{x}_k = \mathbf{x}_k^- + \mathbf{K}_k(y_k - \mathbf{c}_k\mathbf{x}_k^-) \tag{33}$$
$$\mathbf{P}_k = (\mathbf{I} - \mathbf{K}_k\mathbf{c}_k)\mathbf{P}_k^-(\mathbf{I} - \mathbf{K}_k\mathbf{c}_k)^T + \mathbf{K}_k\mathbf{R}\mathbf{K}_k^T \tag{34}$$
$$\widehat{a}_k = \|\mathbf{x}_k\|_2. \tag{35}$$

The Kalman filter is the optimal linear state estimator given white, uncorrelated noise [21]. The process noise especially is unlikely to be white since this will depend on the sample being scanned and overall feedback loop. Additionally, in this case the modeled states are the amplitude of the quadrature sinusoidal signals, not the unknown amplitude itself. The amplitude is found through a nonlinear transformation. Thus, optimality can not easily be concluded.

H. Lyapunov

Here we propose to use an estimation method from [22] based on a Lyapunov proof with a strictly positive real (SPR) pre-filter. It can be proved to be exponentially stable and the convergence rate is determined by the positive gain γ. To the authors' knowledge this approach has not been employed for amplitude estimation in the atomic force microscopy field. Dropping time-dependency for convenience, the estimator can be written as

$$e = s - \mathbf{c}\mathbf{x} \tag{36}$$

$$y = H_{lp}(p)e \tag{37}$$

$$\dot{\mathbf{x}} = \gamma \mathbf{c} y \tag{38}$$

$$\widehat{a} = \|\mathbf{x}\|_2, \tag{39}$$

where $\mathbf{c} = [\sin(\omega_0 t), \cos(\omega_0 t)]$, and $H_{lp}(p)$ is an SPR transfer function such as a first-order low-pass filter. This filter can be exploited to attenuate measurement noise by setting the bandwidth typically close to the desired amplitude estimate bandwidth. The method can easily be tuned either to emphasize low noise (small γ) or fast convergence rate (large γ).

In brief, the method's stability properties can be shown using the Lyapunov function

$$V(\tilde{\mathbf{x}}, \mathbf{z}) = \frac{\tilde{\mathbf{x}}^T \mathbf{P}_c \tilde{\mathbf{x}}}{2} + \frac{\mathbf{z}^T \gamma^{-1} \mathbf{z}}{2} \tag{40}$$

where $\mathbf{P}_c = \mathbf{P}_c^T > 0$, $\tilde{\mathbf{x}}$ is the error between the real and estimated parameter vector $\mathbf{x}$, and $\mathbf{z}$ is the state vector of the state-space representation of y in (37). The SPR property of H_{lp} is exploited in the derivation of the update law (38) such that $\dot{V}$ becomes negative semidefinite. Further analysis provided in [22] guarantees exponential stability of $\tilde{\mathbf{x}}$ to zero, which in turn guarantees $\widehat{a} \to a$ exponentially fast.

IV. SIMULATION RESULTS

The methods described in the previous section have been implemented in Simulink for simulation. A test environment has been setup according to Figure 2 with parameters given in Table I. The phase shift and the amplitude excitation source A represent the cantilever deflection response as the tip interacts with the sample, while the noise source N represents measurement noise.

A few of the methods allow for some tuning, mostly for time constants on low-pass filters and gains. We have tried to optimize for high bandwidth without creating significant overshoot.

The step-response plotted in Figure 3 is simulated without measurement noise for readability. It can be observed that

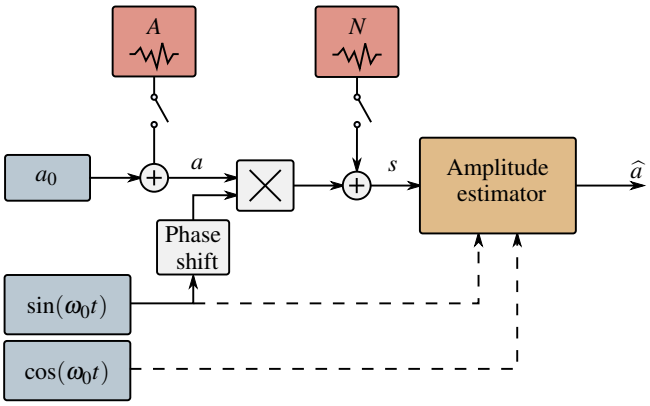

Fig. 2: Block diagram of test environment. A represents the amplitude excitation source, while N represents the measurement noise source.

TABLE I: Simulation Parameters

Oscillation frequency	ω_0	$5000 \cdot 2\pi$ [rad/s]
Oscillation period	T_0	0.2 ms
Measured signal phase	ϕ	15°
Measurement noise std.	σ	2.84 nm
Reference amplitude	a_0	10 nm
Excitation amplitude	a_{exc}	3 nm
Samples per period	S_{pp}	2000
Lyapunov method gain	γ	4×10^4
Lyapunov method filter	$H_{lp}(p)$	$1/(0.6\omega_0^{-1}p + 1)$

the methods update fastest around the peak of the measured signal (twice per period T_0). Most of the information in the signal is located here because the error between two sinusoidal signals of different amplitudes will be greatest here. This will ultimately limit the convergence speed of any amplitude estimator to something close to one half-period.

In Figure 4 it can be seen how well the various methods track sinusoidal changes in amplitude to get an impression of the bandwidth of each method. This plot has been generated using single sinusoidal excitation input of amplitude $a_{exc} = 3\,\text{nm}$ applied at source A seen in Figure 2. For each point in the plot a simulation has been run with a single sinusoidal excitation to the amplitude. The output amplitude in the estimated signal $\widehat{a}$ has been identified using the Goertzel algorithm [23] at the excited frequency. This algorithm effectively computes the discrete Fourier transform at selected frequencies. Gaussian, white measurement noise with standard deviation $\sigma = 2.84\,\text{nm}$ has been added at source N in Figure 2 to approximate a real environment.

To provide an accurate and low-noise amplitude estimate the estimator should attenuate the noise as much as possible. Figure 5 shows the spectral density of the amplitude estimate with measurement noise and constant amplitude. This is closely correlated to the bandwidth of each method, although notably the peak hold and the peak detection method stand out with a very high sensitivity to the noise. These two methods effectively only take one or a few samples respectively per half-period, while all other estimators attenuates the

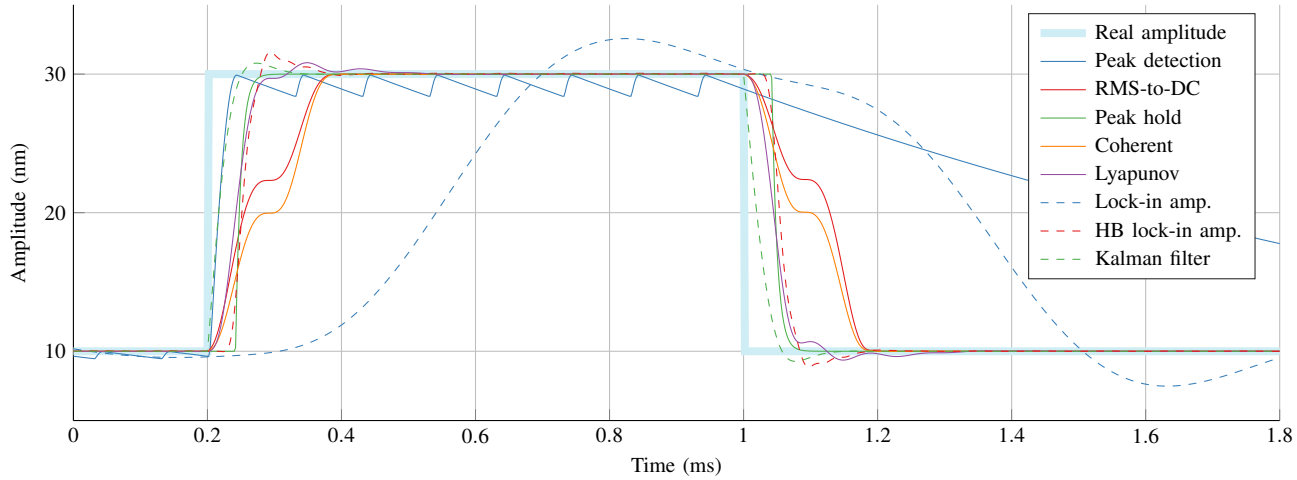

Fig. 3: Step-response of the various amplitude estimation techniques. The majority of the methods changes rapidly twice per period and coincides with peaks of the measured deflection signal. Simulated without measurement noise.

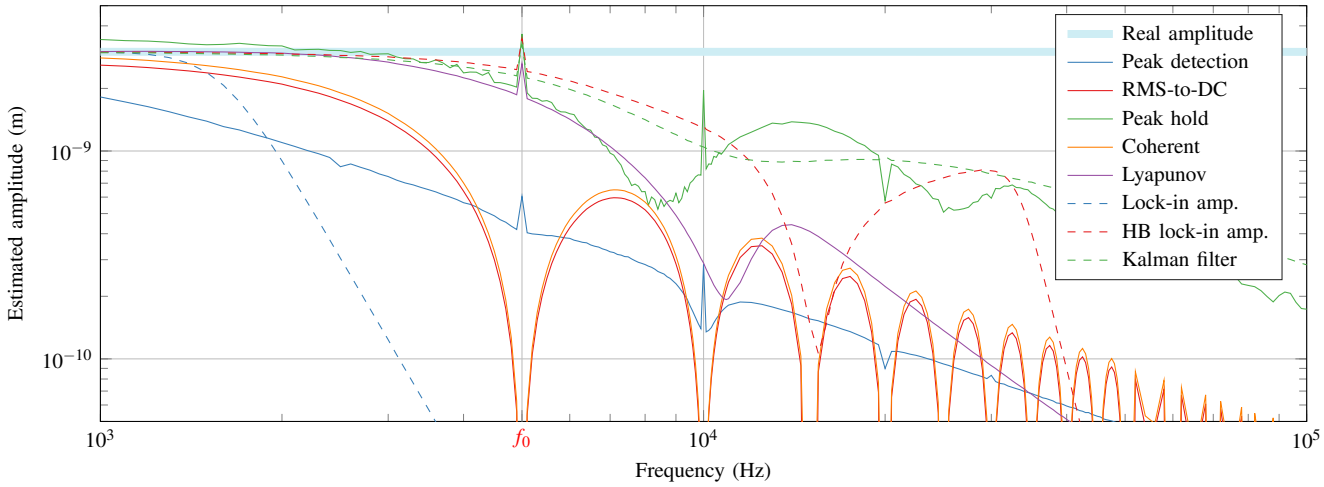

Fig. 4: Estimated amplitude frequency response simulated with measurement noise. This shows the allowable bandwidth for the various amplitude estimation techniques. Simulated using a single sinusoid at the amplitude source A for each data point.

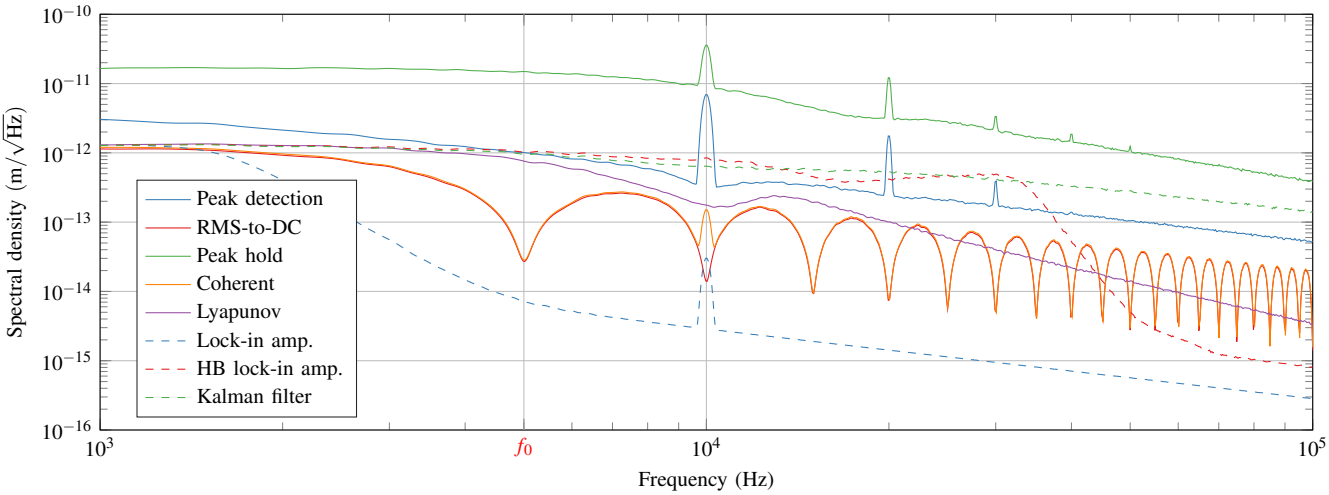

Fig. 5: Spectral density of amplitude estimate with measurement noise and constant amplitude. This shows how well each method attenuates measurement noise; the spectral density should ideally be small for higher frequencies especially above the amplitude response bandwidth.

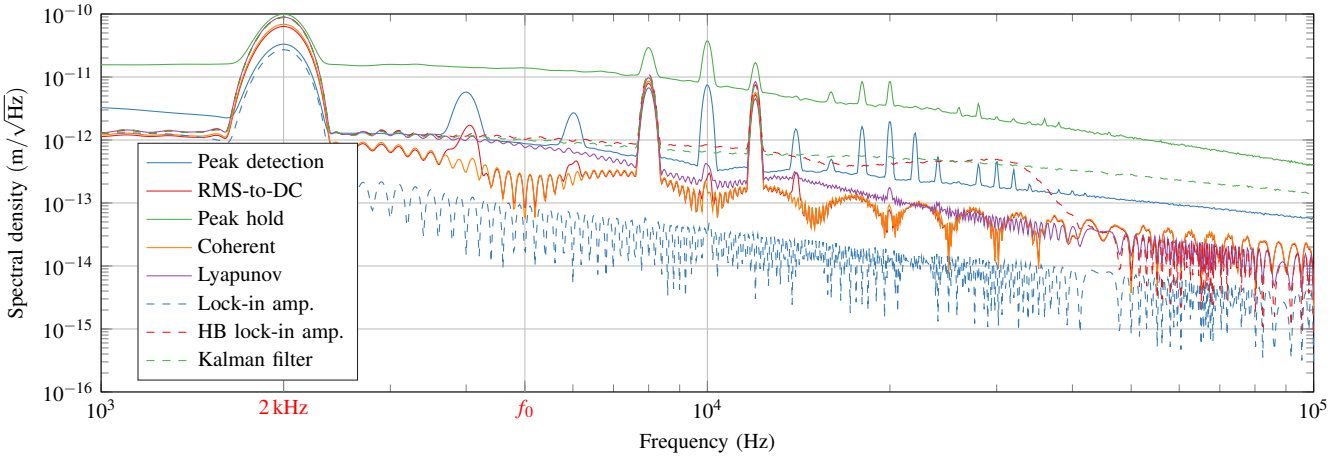

Fig. 6: Spectral density of amplitude estimate with measurement noise and sinusoidal change in the real amplitude with frequency 2 kHz and amplitude 3 nm. The sinusoidal reference gives rise to other harmonics, especially near the 10 kHz range. Harmonics other than the one at 2 kHz are unwanted and represent leakage due to nonlinear effects. Some methods have higher sidelobes than others. In general this is impossible to eliminate in online methods unless by using a strong low-pass filter which would ultimately limit the bandwidth or introduce significant phase lag.

measurement noise by continuously taking several samples per period. These last methods will essentially perform better in terms of noise attenuation with faster sample times, as more samples are taken per period.

The various estimation methods are nonlinear and introduces harmonics in the estimated signal even with a single sinusoidal input amplitude. This can be seen in Figure 6 where a 2 kHz sinusoidal signal with amplitude 3 nm is applied on top of the constant amplitude reference at 10 nm at source *A* seen in Figure 2. Otherwise the setup is exactly the same as in Figure 5. It can be seen that additional harmonics are introduced to the estimates.

Finally, some observed properties of each method as implemented are summarized in Table II.

V. MAKING A CHOICE

Based on the simulation results and general advantages and disadvantages of each method, the following suggestions can be made for the desired properties:

A. Low Complexity

The peak detection, peak hold, and lock-in amplifier methods distinguishes themselves by not requiring reference sinusoidal signals or accurate timing information. This makes them a lot simpler to implement and suitable for analog implementation. The RMS-to-DC implementation in this paper does require accurate knowledge of the oscillation period, although simpler implementations of this method are possible. However, simpler implementations will need to average for longer thus decreasing the bandwidth.

If a simple estimator with high bandwidth is desired, the peak hold method is the clear choice. If accuracy and low noise is preferable and digital implementation is available the RMS-to-DC method described in this paper is recommended. Otherwise a simpler RMS-to-DC method with longer averaging is suitable. Peak detection is possibly the simplest method to implement, but is not suitable for feedback control due to its oscillatory nature from peak to peak, and very low convergence speed as the amplitude decreases. This will magnify the problem of *parachuting* in dynamic mode AFM which is already a challenge for high scanning speeds [5].

B. Low Noise and High Accuracy

If a non-biased estimator is desired, the peak detection especially and the RMS-to-DC method secondly should be avoided. However, for closed-loop control this is rarely a big concern. Response to measurement noise on the other hand will affect the complete control loop. From Table II it can be seen that the peak hold and peak detection methods are especially prone to noise.

All other methods can be tuned or modified to lower their bandwidth and thus attenuate noise. The Kalman filter is possibly the method which will provide the best noise response if tuned correctly by changing the process and measurement noise covariances. The Lyapunov method is easier to tune with a single gain parameter. Since it is less computationally demanding it can run at faster sample rates. This is an advantage since it will reduce the overall noise floor of the system [18].

The coherent and RMS-to-DC methods can be modified to perform amplitude estimation over multiple oscillation periods which will naturally lower the bandwidth, but also the noise floor. However, maintaining a high sample rate can be a challenge for these methods since they need to store more values in memory with increased number of periods.

C. High Imaging Speed

In general there is a clear trade-off between bandwidth and noise. The high-bandwidth lock-in amplifier is the method which seems to give the best trade-off. However, in practice it may struggle with non-perfect phase cancellation resulting

TABLE II: Amplitude estimation properties*.

Technique	Convergence time	Bandwidth (kHz)	Bias (pm)	Standard deviation (pm)	Phase estimation	Reference sinusoidals required	Accurate timing necessary
Peak detection	Exponential (fast up/slow down)	1.4	269	160	No	No	No
RMS-to-DC	Finite time (T_0)	2.9	12	14	No	No	Yes
Peak hold	Exponential (fast) + Constant ($\frac{1}{4}T_0$)	6.1	-3	480	No	No	No
Coherent	Finite time (T_0)	3.1	-5	14	Yes	No	Yes
Lyapunov	Exponential (fast)	5.8	0	19	Yes	Yes	No
Lock-in Amp.	Exponential (slow)	1.8	0	11	Yes	No	No
HB Lock-in Amp.	Exponential (fast)	8.9	7	27	Yes	Yes	No
Kalman filter	Exponential (fast)	7.7	0	29	Yes	Yes	No

*Bandwidth measured using a cantilever frequency of 5 kHz. Bias and standard deviation measured with constant amplitude and measurement noise. The constant convergence time term in peak hold will depend on the signal phase, but average to the listed time for uniformly random phase. Exponential fast/slow: approximated time constant smaller/larger than one oscillation period.

in a frequency component most prominently at $2\omega_0$. Thus a low-pass filter is needed to attenuate this component. The Kalman filter is then possibly the method which gives the highest bandwidth versus noise. It is also the most computationally expensive and challenging to implement. A good trade-off between these two techniques is the Lyapunov based method presented in this paper. The arithmetics involved here is a lot simpler than the Kalman filter since it does not need to calculate the covariance matrix and Kalman gain. This should allow for a faster sample time which may lead to better noise response and higher bandwidth in practice.

VI. DISCUSSION

A well-performing estimator will be able to respond quickly to changes in amplitude while attenuating measurement noise. These two goals are clearly not independent of each other as they are only separated by multiplication of the carrier wave as seen in Figure 2. This means there is a fundamental trade-off between bandwidth and noise. This is also seen by the correlation between the amplitude response in Figure 4 and measurement noise response in Figure 5.

The Kalman filter, and the high-bandwidth lock-in amplifier represents the state-of-the art for high-bandwidth amplitude estimation. The Lyapunov based method presented here is comparable in terms of performance with the additional benefit of ease of implementation. In fact, these three methods seem to be at the limit of what is attainable in terms of bandwidth. Most of the amplitude information in the measured signal is located around the signal peak since the error between two sinusoidal signals of different amplitudes will be greatest here. As a result, the estimation techniques generally converge faster near the peak than near zero values of the signal. Thus, a bandwidth of greater than $2\omega_0$ will be difficult if not impossible to achieve. It is then preferable to add a low-pass filter or otherwise reduce gains in order to attenuate high-frequency measurement noise and disturbances from higher harmonics.

VII. CONCLUSIONS

Several traditional and state-of-the-art methods for amplitude estimation have been implemented and compared. The results allow us to provide clear suggestions for choice of method based on emphasis for either low complexity, low noise, or high imaging speeds. The various methods display vast differences in these properties.

In general there is a clear trade-off between the bandwidth and noise attenuation of the amplitude estimation methods. The Kalman filter is possibly the method which provides the best trade-off. In this paper we present a Lyapunov based method which is comparable in terms of bandwidth and noise attenuation. It is somewhat simpler to implement which may allow for higher sample rates and thus reduced noise floor.

REFERENCES

[1] G. Binnig, C. F. Quate, and C. Gerber, "Atomic Force Microscope," *Phys. Rev. Lett.*, vol. 56, no. 9, pp. 930–933, 1986.

[2] R. Garcia and R. Perez, "Dynamic atomic force microscopy methods," *Surface science reports*, vol. 47, no. 6-8, pp. 197–301, 2002.

[3] Y. Jeong, G. R. Jayanth, S. M. Jhiang, and C.-H. Menq, "Direct tip-sample interaction force control for the dynamic mode atomic force microscopy," *Applied Physics Letters*, vol. 88, no. 20, p. 204102, 2006.

[4] M. R. P. Ragazzon, J. T. Gravdahl, K. Y. Pettersen, and A. A. Eielsen, "Topography and force imaging in atomic force microscopy by state and parameter estimation," in *American Control Conference*, 2015, pp. 3496–3502.

[5] T. Ando, T. Uchihashi, and T. Fukuma, "High-speed atomic force microscopy for nano-visualization of dynamic biomolecular processes," *Progress in Surface Science*, vol. 83, no. 7-9, pp. 337–437, 2008.

[6] B. J. Kenton, A. J. Fleming, and K. K. Leang, "Compact ultra-fast vertical nanopositioner for improving scanning probe microscope scan speed," *Review of Scientific Instruments*, vol. 82, no. 12, pp. 1–8, 2011.

[7] T. Sulchek, R. Hsieh, J. D. Adams, G. G. Yaralioglu, S. C. Minne, C. F. Quate, J. P. Cleveland, A. Atalar, and D. M. Adderton, "High-speed tapping mode imaging with active Q control for atomic force microscopy," *Applied Physics Letters*, vol. 76, no. 11, p. 1473, 2000.

[8] M. W. Fairbairn, S. O. R. Moheimani, and A. J. Fleming, "Q Control of an Atomic Force Microscope Microcantilever : A Sensorless Approach," *Journal of Microelectromechanical Systems*, vol. 20, no. 6, pp. 1372–1381, 2011.

[9] N. Kodera, M. Sakashita, and T. Ando, "Dynamic proportional-integral-differential controller for high-speed atomic force microscopy," *Review of Scientific Instruments*, vol. 77, no. 8, p. 083704, 2006.

[10] T. Ando, "High-speed atomic force microscopy coming of age," *Nanotechnology*, vol. 23, no. 6, p. 062001, 2012.

[11] T. Ando, N. Kodera, E. Takai, D. Maruyama, K. Saito, and A. Toda, "A high-speed atomic force microscope for studying biological macromolecules," *Proceedings of the National Academy of Sciences*, vol. 98, no. 22, pp. 12 468–12 472, 2001.

[12] K. S. Karvinen and S. O. R. Moheimani, "A high-bandwidth amplitude estimation technique for dynamic mode atomic force microscopy," *Review of Scientific Instruments*, vol. 85, no. 2, p. 023707, 2014.

[13] K. S. Karvinen, "Control and Estimation Techniques for High-Bandwidth Dynamic Mode Atomic Force Microscopy," Ph.D. dissertation, University of Newcastle, 2014.

[14] M. G. Ruppert, K. S. Karvinen, S. L. Wiggins, and S. O. R. Moheimani, "A Kalman Filter for Amplitude Estimation in High-Speed Dynamic Mode Atomic Force Microscopy," *Control Systems Technology, IEEE Transactions on*, vol. 24, no. 1, pp. 276–284, 2016.

[15] D. Y. Abramovitch, "Low latency demodulation for Atomic Force Microscopes, Part I efficient real-time integration," in *American Control Conference*, 2011, pp. 2252–2257.

[16] H.-J. Butt and M. Jaschke, "Calculation of thermal noise in atomic force microscopy," *Nanotechnology*, vol. 6, no. 1, pp. 1–7, 1995.

[17] A. J. Fleming and K. K. Leang, *Design, Modeling and Control of Nanopositioning Systems*, ser. Advances in Industrial Control. Cham: Springer International Publishing, 2014.

[18] R. G. Lyons, *Understanding Digital Signal Processing*, 3rd ed. Upper Saddle River, NJ: Prentice Hall, 2010.

[19] P. Stoica, H. Li, and J. Li, "Amplitude estimation of sinusoidal signals: Survey, new results, and an application," *IEEE Transactions on Signal Processing*, vol. 48, no. 2, pp. 338–352, 2000.

[20] J. Kokavecz, Z. Tóth, Z. L. Horváth, P. Heszler, and Á. Mechler, "Novel amplitude and frequency demodulation algorithm for a virtual dynamic atomic force microscope." *Nanotechnology*, vol. 17, no. 7, pp. S173–S177, 2006.

[21] D. Simon, *Optimal State Estimation*. New York: Wiley, 2006.

[22] P. A. Ioannou and J. Sun, *Robust adaptive control*. Upper Saddle River, NJ: Prentice Hall, 1996.

[23] J. G. Proakis and D. G. Manolakis, *Digital signal processing : principles, algorithms, and applications*, 3rd ed. Englewood Cliffs, NJ: Prentice Hall, 1996.